Nuclear Engineering and Design 239 (2009) 526–540

Contents lists available at ScienceDirect

Nuclear Engineering and Design

journal homepage: www.elsevier.com/locate/nucengdes

Thermal–hydraulic characteristics of a single-phase natural circulation loop with water and Al_2O_3 nanofluids

A.K. Nayak*, M.R. Gartia, P.K. Vijayan

Reactor Engineering Division, Bhabha Atomic Research Centre, Trombay, Mumbai 400085, India

ARTICLE INFO

Article history:
Received 11 April 2008
Received in revised form
12 November 2008
Accepted 20 November 2008

ABSTRACT

A natural circulation system operates on the basis of natural laws like gravity and buoyancy. Although natural circulation is a benign gift of nature for applications to several heat removal systems due to their simplicity in design, elimination of hazards related to pumps, better flow distribution, cost reduction, etc. however, the potential threat of flow instabilities still eludes for its wide applications. Although addition of local losses (orificing) may suppress instabilities, however, it is accompanied by significant flow reduction which is detrimental to the natural circulation heat removal capability. In this paper, we have demonstrated experimentally, with nanofluids, not only the flow instabilities are suppressed but also the natural circulation flow rate is enhanced. The increase in steady natural circulation flow rate due to addition of nanoparticles is found to be a function of its concentration in water. The flow instabilities are found to occur with water alone only during a sudden power addition from cold condition, step increase in power and step decrease in power (step back conditions). With a small concentration of Al_2O_3 nanofluids, these instabilities are found to be suppressed significantly.

© 2008 Elsevier B.V. All rights reserved.

1. Introduction

With the demand for energy continues to grow globally, there is a need to make heat transfer equipment more energy efficient. At one hand, the exponential growth of electronics, communication and computer technology and their choice to go for miniaturization has put added pressure on the designer to create efficient thermal management devices for these systems. On the other hand, large devices (such as space vehicles, transportation trucks) and new emerging energy technology (such as fuel cells) are also looking for more efficient cooling systems with greater cooling capacities and decreased sizes. Also the renewed stress on producing green energy has put back nuclear energy on the energy mix. To assure that nuclear power remains a viable option in meeting energy demands, the new designs of nuclear power plants demand more economy and efficiency.

Thus, big or small, old energy system or new energy system, an enhanced cooling technology is the need of the hour. This need can be met in two ways: *introducing new designs for cooling devices*, such as microchannels and miniature cryodevices, and *enhancing the heat transfer capability of the fluid itself* (Das et al., 2006). Heat transfer fluids such as water, mineral oil and ethylene glycol play a vital role in many industrial processes, including power generation, chemical processes, heating or cooling processes, and microelectronics. The poor heat transfer properties of these common fluids compared to most solids is a major obstacle to achieve higher heat transfer capabilities using these conventional fluids.

An innovative idea for enhanced heat transfer in a fluid was to suspend ultrafine solid particles in it for improving the thermal conductivity of the fluid (Maxwell, 1881). Many types of particle, such as metallic, non-metallic and polymeric, can be added into fluids to form slurries. However, the usual slurries, with suspended particles in the order of millimeters or even micrometers may cause some severe problems. The abrasive action of the particles causes the clogging of flow channels, erosion of pipelines and their momentum transfers into an increase in pressure drop in practical applications. Furthermore, they often suffer from instability and rheological problems (Daungthongsuk and Wongwises, 2007). In particular, the particles tend to settle rapidly. Thus, although the slurries give better thermal conductivities, they are not practical.

The use of particles of nanometer dimension was first pioneered by a research group at the Argonne National Laboratory around a decade ago. Choi (1995) was probably the first one who called the fluids with particles of nanometer dimensions 'nanofluids'. Nanofluids are stable colloidal suspensions of nanoparticles, nanofibers, or nanocomposites in common, base fluids, such as water, oil, ethylene glycol mixtures (antifreeze), polymer solutions, etc. Nanoparticles are very small, nanometer-sized particles with dimensions usually less than 100 nm (nanometers). The smallest nanoparticles, only a few nanometers in diameter, contain only a

* Corresponding author. Tel.: +91 22 25591557; fax: +91 22 25505151.
E-mail address: arunths@barc.gov.in (A.K. Nayak).

0029-5493/$ – see front matter © 2008 Elsevier B.V. All rights reserved.
doi:10.1016/j.nucengdes.2008.11.014

Nomenclature

A	flow area (m^2)
b	constant in Eq. (2)
C_p	specific heat (J/(kg K))
D	hydraulic diameter (m)
f	Darcy–Weisbach friction coefficient
g	gravitational acceleration (m/s^2)
Gr_m	modified Grashof number ($D^3\rho^2\beta g\,\Delta T_r/\mu^2$)
H	loop height (m)
k	thermal conductivity (W/(m K))
l_i	dimensionless length (L_i/L_t)
L	length (m)
p	constant in Eq. (2)
Q	total heat input rate (W)
Re	Reynolds number ($DW/A\mu$)
T	temperature (K)
ΔT_r	reference temperature difference ($QH/A\mu C_p$) (K)
W	mass flow rate (kg/s)
Δz	center line elevation difference between cooler and heater (m)

Greek symbols

β	thermal expansion coefficient (K^{-1})
θ	dimensionless temperature $(T-T_s)/(\Delta T_h)_{ss}$
μ	dynamic viscosity ($N\,s/m^2$)
ρ_0	reference density (kg/m^3)

Subscripts

h	heater
hl	hot leg
r	reference value
ss	steady state
t	total

few thousand atoms. These nanoparticles can possess properties that are substantially different from their parent materials (Kostic and Choi, 2006).

Coming back to natural circulation, natural circulation loops are extensively used in several industries. Single-phase systems are used in the solar water heaters, transformer cooling and nuclear reactor core cooling. For reactor application, single-phase natural circulation is used for decay heat removal in PWRs, VVERs and PHWRs during upset conditions like pumping power failure. It is also used in district heating reactors (Samoilov and Kurachenkov, 1997) and certain low power reactors like CAREM (Delmastro, 2000) as the normal mode of core cooling. The primary function of a natural circulation loop is to transport heat from a source to a sink. The heat transport capability of natural circulation loops is directly proportional to the flow rate it can generate. Hence, the steady state flow rate is directly associated with the efficiency of the single-phase natural circulation systems.

Natural circulation systems are susceptible to several types of instabilities. Although, the heat transport capability does not break down completely during instability, it is undesirable in an operating reactor as it can lead to large amplitude flow and power oscillations. It can also lead to forced mechanical vibrations, premature occurrence of critical heat flux (CHF), problems in reactor control and operation. Strictly speaking, natural circulation (NC) reactor systems shall be designed to avoid all known instabilities.

Both static and dynamic instabilities are observable in single-phase natural circulation systems. The static instability is usually associated with multiple steady states in different flow directions. It is observed in asymmetrically heated single channel or unequally heated parallel channel systems (Chato, 1963). In addition, single-phase natural circulation systems exhibit a dynamic instability (Welander, 1967) of the density wave type. Welander (1967) has also proposed a mechanism for this instability. Experimentally instabilities in a single-channel toroidal loop were first observed by Creveling et al. (1975). The earliest experimental work in a rectangular loop with vertical heater and cooler by Holman and Boggs (1960) did not study the instability. Subsequent studies in rectangular loops by Huang and Zelaya (1988), Misale et al. (1991), Bernier and Baliga (1992) and Ho et al. (1997) also concentrated on the steady-state behavior. Vijayan et al. (1992) observed instability for the first time in a rectangular loop while experimenting with uniform diameter loops. Generally, density wave instability is observed in single-phase systems with low length to diameter (L/D) ratios. In fact it is not yet observed in systems with L/D ratio greater than 300. In most nuclear reactors, this ratio is of the order of a few thousands and hence single-phase density wave instability is not normally observed in reactor systems (Vijayan et al., 2008). However, even in a reactor system instability can be observed with external influences such as a throughflow superimposed on single-phase natural circulation (Vijayan and Date, 1992).

The purpose of this research paper is concerned with the use of Al_2O_3 nanofluids to suppress the instabilities in a single-phase natural circulation loop induced by a heating–cooling system. Experiments were demonstrated by running the system to compare the pressure drop and natural circulation flow rate with water and that with nanofluids at different concentrations. It was presented in this work that the nanofluids is able to suppress the instability and enhance the fluid flow according to the measurement of pressure drop and flow rate of the fluid. The main focus of this research was to develop a technology to get rid of the flow instabilities generally associated with the natural circulation loop without degrading the natural circulation flow rate.

2. Experimental facility

Experiments were conducted in a natural circulation loop with geometry as shown in Fig. 1. The test facility resembles rectangular in geometry with circular flow cross-section area. The pipes are made of borosilicate glass with inner diameter of around 26 mm. Important dimensions of the loop are shown in Fig. 1. The loop was

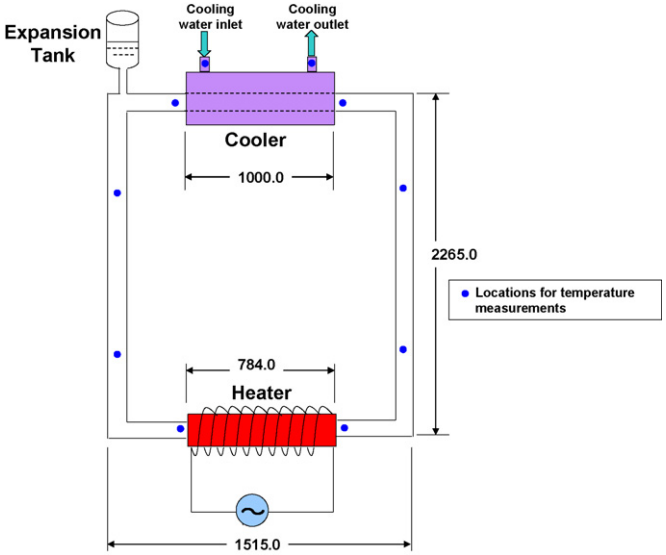

Fig. 1. Schematic of experimental facility.

heated with electric wire which was wrapped around uniformly on the outer surface of the glass tube in the bottom horizontal leg. It was cooled at the top through a tube-in-tube type heat exchanger with tap water flowing through the annulus. An expansion tank was provided at the topmost elevation to accommodate the volumetric expansion of the fluid. It also ensures that the loop remains full of water. Thermocouples were installed at different positions in the loop to measure the instantaneous local temperature. The flow rate was measured using a differential pressure transducer installed in the horizontal leg of the loop. The instruments were connected to a data acquisition system which could scan all the channels in less than 1 s. The secondary side cooling water flow rate was measured with the help of a rotameter. The loop was insulated to minimize the heat losses to the ambient. The measurement accuracy was 0.4% (±1.1 °C) for thermocouples, ±0.25% for flow rate and ±0.5% of the span (0–1250 W) for power and pressure drop (−150 to −150 Pa). Experiments were conducted at different powers which are typical to that of a power raising and setback phenomena in any power generating system. The power to the test section was varied by using a DC variac.

2.1. Preparation of nanofluids

An aqueous solution of nanofluids was prepared by adding desired concentration (by weight) of Al_2O_3 (Alumina) nanopowder of particle size 40–80 nanometer and 99.7% purity to the water in the loop. The reason for using Al_2O_3 nanopowder is the fact that the thermo-physical characteristics of the base fluid (water) is most widely known and the thermal property of water–Al_2O_3 nanofluids for different particle concentration has already been studied (Das et al., 2003a). To prevent the particles from agglomerating and settling, the suspension was sonicated in an ultrasonic bath. The dispersion of the particle was first done by mixing the required volume of powder in a chemical measuring flask with distilled water and then using ultrasonic vibration to disperse it. After making a proper mixture, the flask was kept again under ultrasonic vibration for about 4 h, which is a sufficient time to ensure stable particle dispersion in water without agglomeration (Das et al., 2003b). The size of nanoparticles in powder form was characterized by transmission electron microscope (TEM). The colloidal particle size (sample taken after sonication) was further characterized by dynamic light scattering technique.

The settling velocity was calculated from a balance of buoyancy and viscous forces and using the Stokes law for the viscous resistance (Buongiorno, 2006). The settling velocity was found to be $\sim 1.043 \times 10^{-8}$ m/s for the mean particle size of 60 nm as used in this experiment (see Appendix for details). In fact, this velocity is negligibly small as compared to the momentum of the fluid due to natural convection. Hence, the question of settling of nanoparticles during the tests does not arise especially for the long duration experiments.

2.2. Experimental procedure

2.2.1. Basic procedure

The primary loop was filled with tap water. To drive out the air bubbles, the filling flow was continued for some more time with pulsing. To remove the dissolved gases in the water, the loop was run under natural circulation condition at a small power for some time (1–2 h). This procedure was followed in all the tests to drive out the dissolved gases. Before the experiment, the secondary cooling water flow rate was set at the required value. Sufficient time (1–2 h) was given for the test loop to stabilize at room temperature without heating. Then power was switched on and actual recording of data began.

2.2.2. Steady-state test procedure

When steady initial conditions were reached, the reading was noted with zero power. Then the heater was put on and set at the required power using the DC controlled heating Variac. At the steady-state condition (which can be observed from the trend of the pressure drop data and temperature variation in the graphical display mode on the data acquisition system), all the temperatures and pressure drop data were collected. Then the power was increased in steps of 50 W and allowed to attain the steady state. The same procedure was repeated till the power reached 450 W. Repeatability of the test results was also checked.

2.2.3. Procedure for the stability tests

The instability threshold was found to be dependent on heat addition paths. The scenarios for the following heat addition paths were studied:

1. start-up from stagnant conditions;
2. sudden power raising from an initial stable steady-state conditions;
3. instability behavior during a power step back process.

During all the tests the cooling water flow rate (1 l/min) and its inlet temperature (around 32 °C) were kept constant. The fluctuation in the controlled coolant flow rate was within ±3% of the set value. A brief experimental procedure is given below for each of the tests.

2.2.4. Start-up from stagnant conditions

The experimental procedure consisted of suddenly switching on the heater when the fluid was stagnant at uniform initial temperature throughout the loop. To achieve uniform initial temperature, the cooling water was valved-in at least half an hour before the actual test. The system was allowed to operate until the flow was stable. The primary objective of these tests was to obtain the threshold power below which the system can be started up without encountering instability with sudden increase in power from initial stagnant condition. These experiments were conducted with water alone and repeated with the addition of 1% by weight of nanofluids.

2.2.5. Power raising from stable steady-state conditions

In these experiments an initial stable steady state with unidirectional flow was achieved first. For achieving the initial steady state, the procedure as mentioned above was followed. After achieving the initial steady state, a step increase in power was given. Sufficient time was given to achieve a new steady state or oscillatory behavior. If the system remains stable another step increase in power was given. The process was repeated till instability was observed. The objective was to determine the threshold value up to which power can be raised smoothly (in single or several steps) without encountering instability. Again, these experiments were conducted with water alone and repeated with addition of 1% by weight of the nanofluids.

2.2.6. Instability behavior during power step back

Here an initial oscillatory condition was established first. To establish this condition, the same procedure as that stated above was followed. After the oscillatory behavior sets in sufficient time was allowed for the initial transients to die out. Then a step decrease in power was given. Sufficient time was allowed to achieve a new state (stable or oscillatory). The test was repeated for different initial oscillatory flow conditions. The objective of these tests was to study the difference in flow instability characteristics during power raising and step back condition for the corresponding heater power.

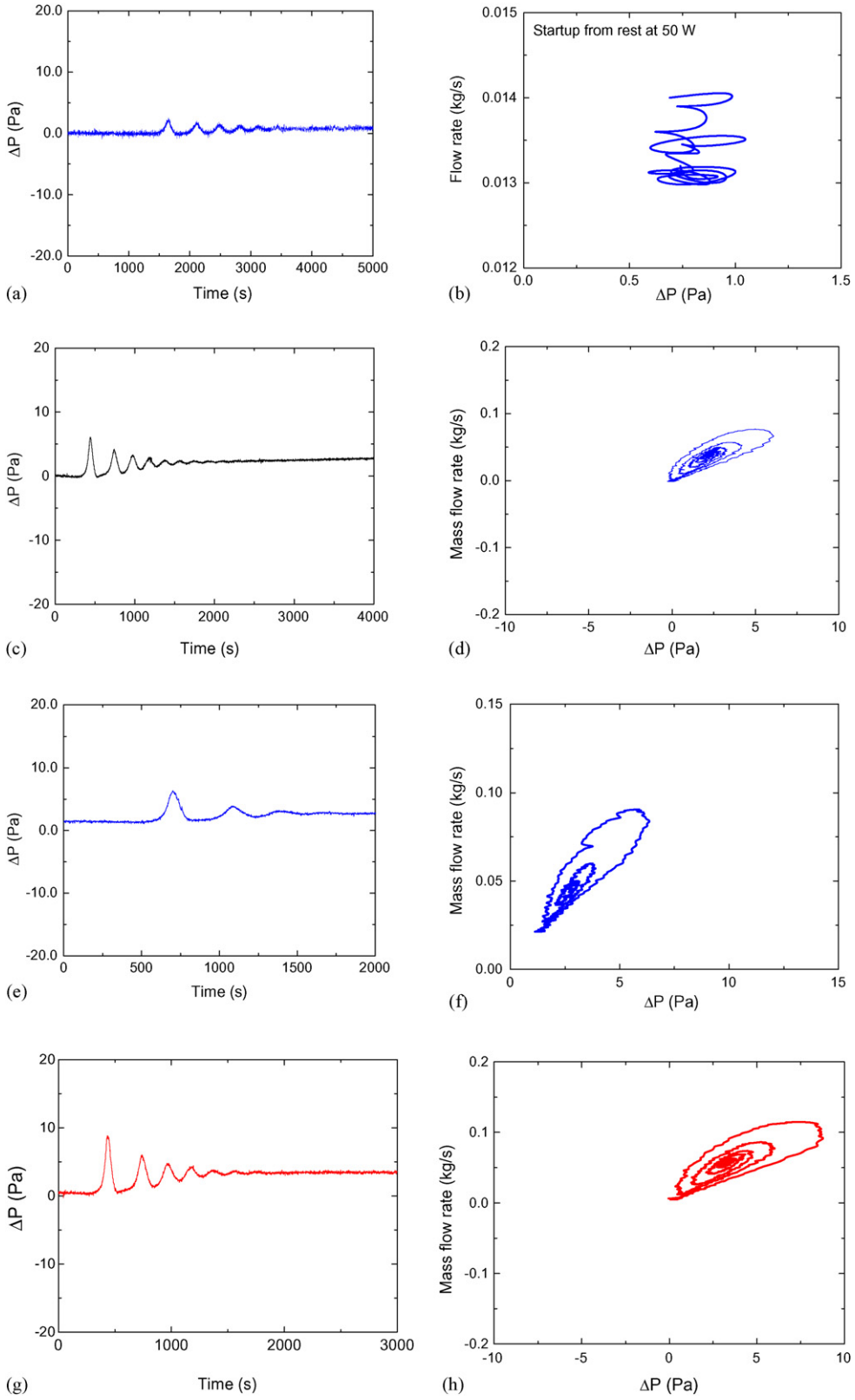

Fig. 2. Comparison of flow behavior at 50 W with water and with nanofluids. (a) Start-up at 50 W without nanoparticles, (b) phase plot for start-up at 50 W without nanoparticles, (c) start-up at 150 W without nanoparticles, (d) phase plot for start-up at 150 W without nanoparticles, (e) start-up at 50 W with nanoparticles, (f) phase plot for start-up at 50 W with nanoparticles, (g) start-up at 150 W with nanoparticles and (h) phase plot for start-up at 150 W with nanoparticles.

These experiments were conducted with water alone as well as with the nanofluids (concentration of 1% by wt.).

3. Experimental observations

3.1. Start-up from stagnant conditions

The different flow regimes observed during the experiments can be listed as below:

(a) steady unidirectional flow;
(b) periodic unidirectional pulsing flow;
(c) periodic bidirectional pulsing flow;
(d) oscillatory flow with chaotic switching between unidirectional and bidirectional pulsing;
(e) compound single phase–two phase instability with bidirectional pulsing.

3.1.1. Steady unidirectional flow

Fig. 2 depicts a typical history of thermal–hydraulic characteristics of the natural circulation loop with water alone for different heat addition conditions. A comparison of each of the characteristics found with water and repeated with nanofluids has been presented in the same figure also.

The observed natural circulation behavior with water alone following the addition of 50 W from stagnant condition leads to a stable steady state as shown in Fig. 2a. Stable unidirectional flow is represented by fixed point on the phase plots (Fig. 2b). The time lag between the heating process and the subsequent generation of buoyancy force results in the initial oscillatory behavior, which gets damped with time. This behavior is observed until the power is

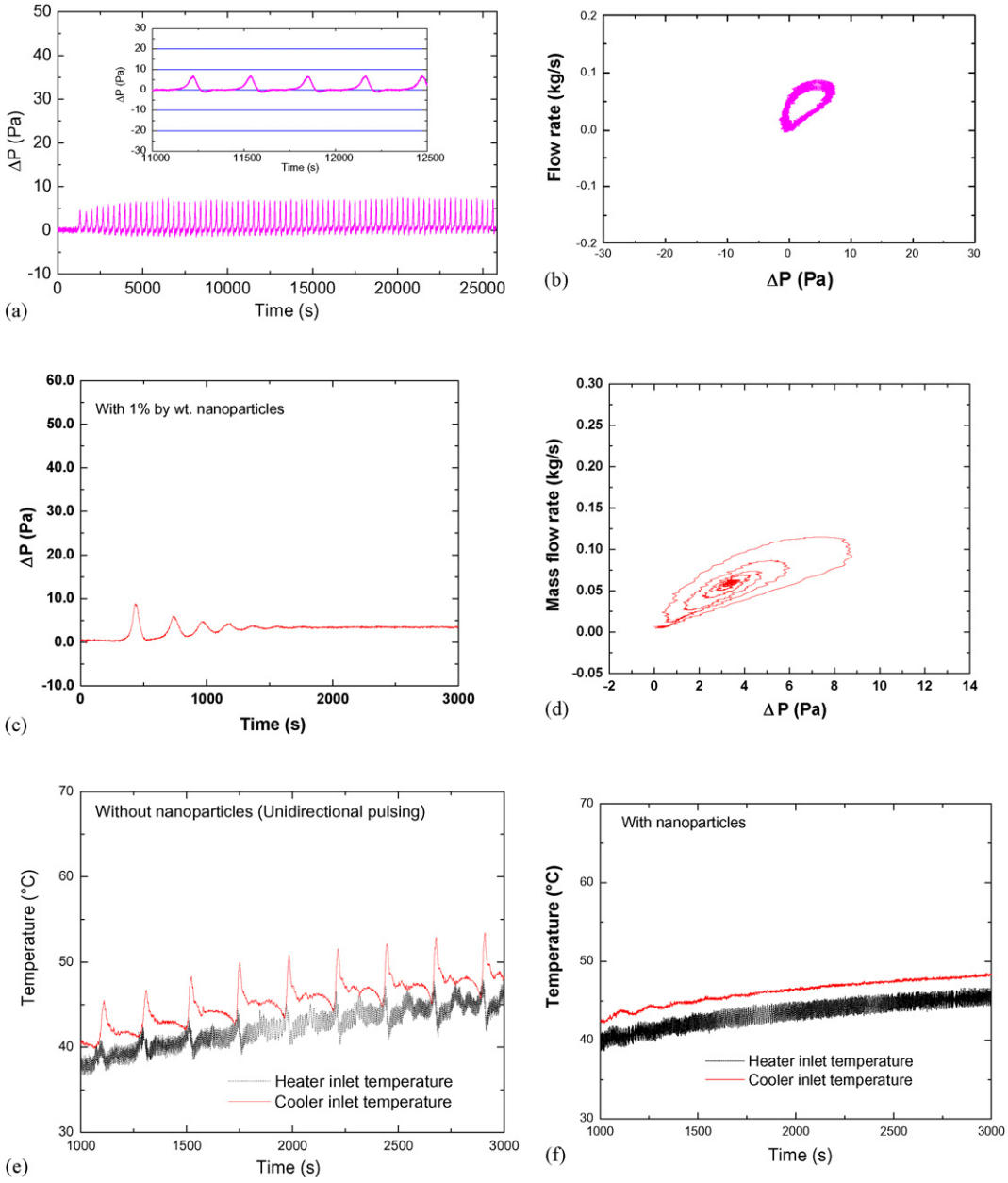

Fig. 3. Comparison of flow behavior at 175 W with water and with nanofluids. (a) Start-up at 175 W without nanoparticles, (b) phase plot for start-up at 175 W without nanoparticles, (c) start-up at 175 W with nanoparticles, (d) phase plot for start-up at 175 W with nanoparticles, (e) temperature variation with water alone and (f) temperature variation with nanofluids.

below 150 W (Fig. 2c and d). The corresponding flow behavior with nanofluids is shown in Fig. 2e and f. The steady-state flow was found to be higher than that with water alone. The flow rate in the phase plots was computed from the measured pressure drop as shown in Appendix.

3.1.2. Periodic unidirectional pulsing flow

As the name suggests, unidirectional pulsing is characterized by periodic high flow pulses in the same direction followed by a period of near stagnant flow so that it appears to be repetitive flow initiations and is observed only at low powers. The steady unidirectional oscillatory flow is observed (Fig. 3a) when the heater power is suddenly increased to about 175 W from initial stagnant condition. The flow is found to reduce to zero following the pulse. Due to sudden increase in power, a hot pocket is created in the heater which rises with a high velocity while climbing in the riser (observed as a pulse). The hot pocket is unable to get diffused while passing through the cooler due to its low residence time (high velocity). As a result the net buoyancy force reduces to almost zero when the hot plug of fluid descends along the cold leg. On the phase space (ΔP–W plane), unidirectional pulsing portrays a bean shaped limit cycle (Fig. 3b). The same experiment was repeated with 1% by wt. concentration of nanofluids. The flow was found to be stable at that power and the flow behavior is shown in Fig. 3c. The corresponding phase plot is shown in Fig. 3d. The temperature variation at the inlet of heater and the inlet of cooler are shown in Fig. 3e and f with water alone and with nanofluids, respectively. The temperature at the inlet of heater and cooler are found to oscillate out-of-phase when the loop was filled with water alone.

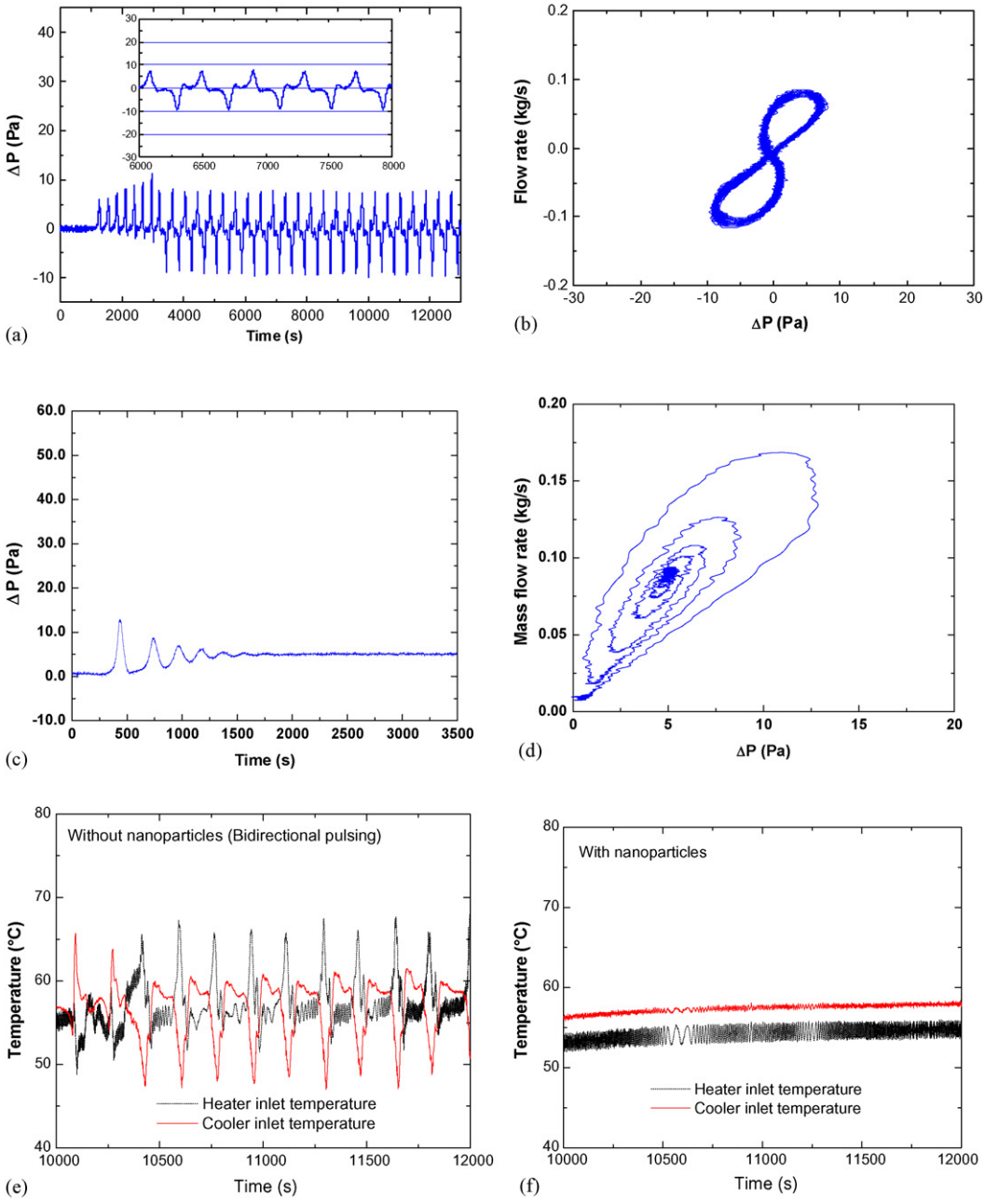

Fig. 4. Comparison of flow behavior at 300 W with water and with nanofluids. (a) Start-up at 300 W without nanoparticles, (b) phase plot for start-up at 300 W without nanoparticles, (c) start-up at 300 W with nanoparticles, (d) phase plot for start-up at 300 W with nanoparticles, (e) temperature variation with water alone and (f) temperature variation with nanofluids.

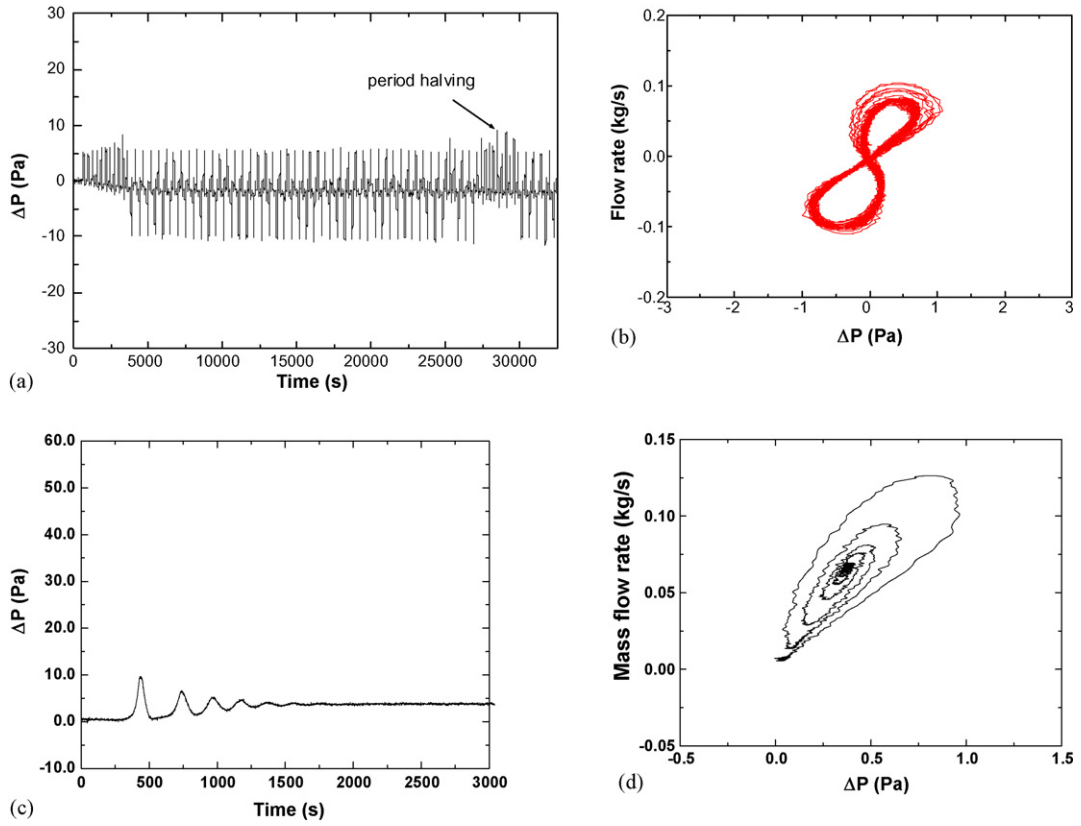

Fig. 5. Comparison of flow behavior at 220 W with water and with nanofluids. (a) Start-up at 220 W without nanoparticles, (b) phase plot for start-up at 220 W without nanoparticles, (c) start-up at 220 W with nanoparticles and (d) phase plot for start-up at 220 W with nanoparticles.

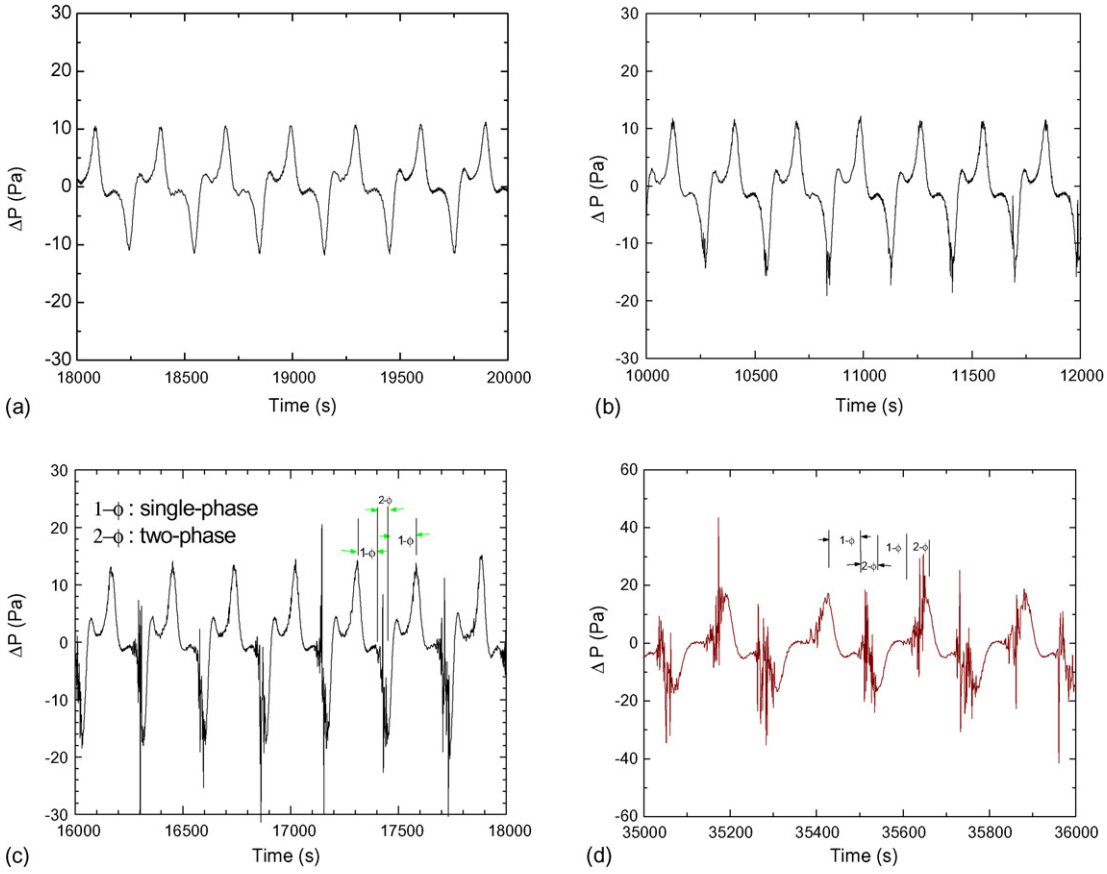

Fig. 6. Unstable oscillatory behavior with subcooled boiling at different powers. (a) Single-phase bidirectional pulsing at 380 W, (b) sporadic subcooled boiling at 430 W, (c) bidirectional pulsing with subcooled boiling at 518 W and (d) bidirectional pulsing with subcooled boiling at 600 W.

3.1.3. Periodic bidirectional pulsing flow

Bidirectional pulsing is characterized by the occurrence of alternate clockwise and anticlockwise flow pulses. For a sudden power input of 300 W added to the stagnant liquid, a periodic bidirectional pulsing is observed after some initial unidirectional oscillation (whose amplitude increases with time) with water alone (Fig. 4a). During the bidirectional pulsing, repeated flow reversals occur along with alternate forward and reverse flow pulses (Fig. 4a). On the phase space (ΔP–W plane), bidirectional pulsing portrays a dumbbell shaped limit cycle (Fig. 4b). However, stable steady-state flow was found with 1% by wt. concentration of nanofluids at 300 W and the flow behavior is shown in Fig. 4c. The corresponding phase plot is shown in Fig. 4d. The temperature variation at the inlet of heater and the inlet of cooler are shown in Fig. 4e and f with water alone and with nanofluids, respectively. The temperature at the inlet of heater and cooler are found to oscillate out-of-phase when the loop was filled with water alone.

3.1.4. Oscillatory flow with chaotic switching between unidirectional and bidirectional pulsing

Between unidirectional pulsing and bidirectional pulsing, a regime with chaotic switching between unidirectional and bidirectional pulsing (intermittency) is observed at 220 W (Fig. 5a) when the loop was filled with water alone. The phase portrait for the unstable flow regime with chaotic switching shows a dumbbell shape with a spread around the periphery (Fig. 5b). The same experiment was repeated with 1% by wt. concentration of nanofluids. The flow was found to be stable at that power and the flow behavior is shown in Fig. 5c. The corresponding phase plot is shown in Fig. 5d.

3.1.5. Compound single phase–two phase instability with bidirectional pulsing

At higher powers, the instability continues in the bidirectional pulsing mode superimposed by subcooled boiling. During the low flow part of the oscillation cycle bubbles are formed near the top surface of the heater outlet, which are stationary to start with. When these bubbles are released high ΔP occurs since two-phase ΔP is significantly larger than single-phase ΔP. Boiling is indicated by the occurrence of sharp peaks in the ΔP due to bubble release, which was also confirmed by visual observation. For the sake of comparison, a typical non-boiling case is shown in Fig. 6a. Due to the sudden increase of flow when the bubbles enter the vertical leg boiling is suppressed (Fig. 6b–d). However, with nanofluids this regime was not observed (Fig. 7) and the flow was found to be stable.

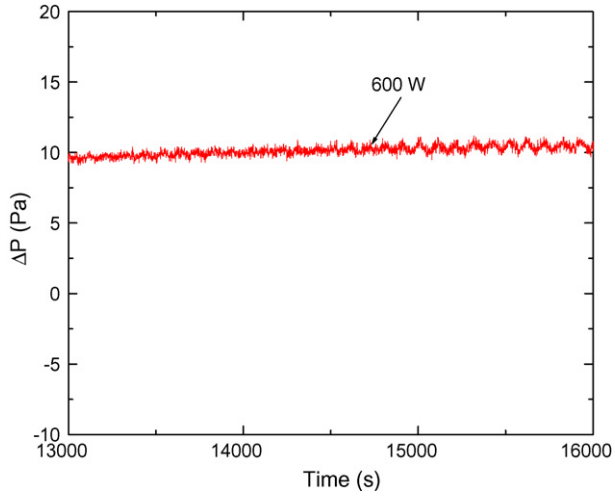

Fig. 7. Flow behavior with nanofluids at 600 W.

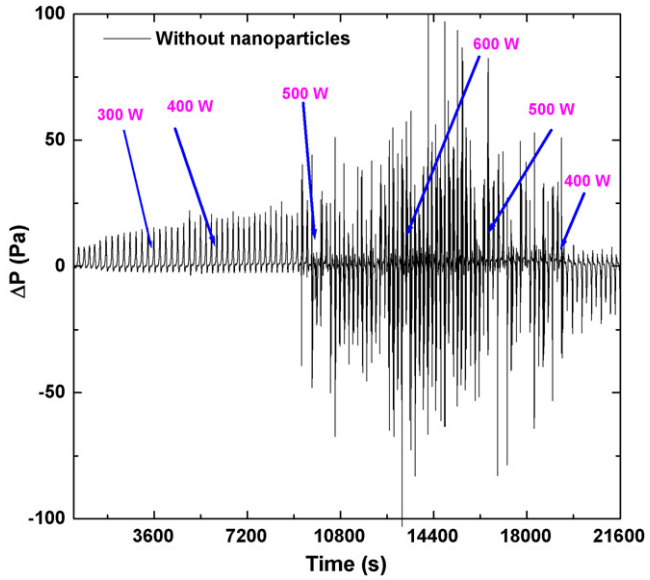

Fig. 8. Oscillatory flow with chaotic switching between unidirectional and bidirectional pulsing: start-up at 300 W and power raising to 600 W.

3.2. Sudden power rise and step back experiments from initial oscillatory condition

An example of the flow instability behavior of the natural circulation loop during a power raising and step back process is shown in Fig. 8 when the loop was filled with water alone. In this case, the fluid was heated from an initial power of 300 W in steps of 100 W, and the instabilities were observed at 300 W. The amplitude of oscillations kept on increasing with rise in power. At 600 W, a power step back experiment was conducted to illustrate the instability behavior during a step back process. The power was reduced to 400 W from 600 W in steps of 100 W. The flow instabilities were found to be sustained and their characteristics are different for the corresponding powers during the power raising process (Fig. 9a–l). At high power (greater than 500 W), subcooled boiling occurs which leads to the formation of cusps in the dumbbell shaped trajectory (see Fig. 9f). Both the time series and the phase plots show an increasingly chaotic behavior with increase in power (Fig. 9f and h). The temperature variation at the inlet of heater and cooler with water alone and with nanofluids is shown in Fig. 10 at 600 W. Typically at this power compound single phase–two phase instability with bidirectional pulsing is observed with water alone. The experiment was repeated with Al_2O_3 nanoparticles. As seen from Fig. 11, it was found that the instabilities are totally suppressed with nanofluids.

Similar behavior was observed when a sudden increase in power to 500 W was given and the power was increased further to 600 W in step of 100 W. Subsequently the step back experiment was conducted by reducing the power to 400 W in steps of 100 W. Fig. 12a shows the flow behavior for the above power transient with water alone. Fig. 12b shows the variation of flow with nanofluids for the same power history. It can be seen that the instabilities are not observed with nanofluids.

3.3. Gradual power rise from stable initial conditions

Typical results for the occurrence of instability for gradual power raising from initial stable steady state are shown in Fig. 13a and b when the loop was filled with water alone. Unlike the previous case, wherein instabilities are observed when the power was suddenly increased to 300 W, in this case no instabilities were found even

up to 450 W. However, at 600 W, flow instabilities developed with growth of small amplitude oscillations. This suggests that the instability phenomena is highly non-linear and path dependent. The corresponding flow behavior with nanofluids is shown in Fig. 13c. Instabilities are not observed with nanofluids even at high power. The stable flow is represented by fixed point on the phase plots as shown in Fig. 13d.

3.4. Time period of oscillation

Fig. 14 shows the time period of oscillation as a function of heater power for all the oscillatory cases. During the unidirectional flow oscillations the time period is found to reduce exponentially with increase in power. Whenever the flow regime switches from unidirectional to bidirectional pulsing, the oscillation period increases (Fig. 14). Period doubling is a usual step for transition to chaos (Kapitaniak, 2000). A near period doubling is observed for low power experiments.

3.5. Parametric studies

3.5.1. Effect of concentration of nanoparticles on steady-state flow

Steady-state experiments were conducted with water and different concentration of nanoparticles (0.3–2% by wt.). It was found that the natural circulation flow rates increase with increase in concentration of nanoparticles (Fig. 15a). Fig. 15b shows that the flow

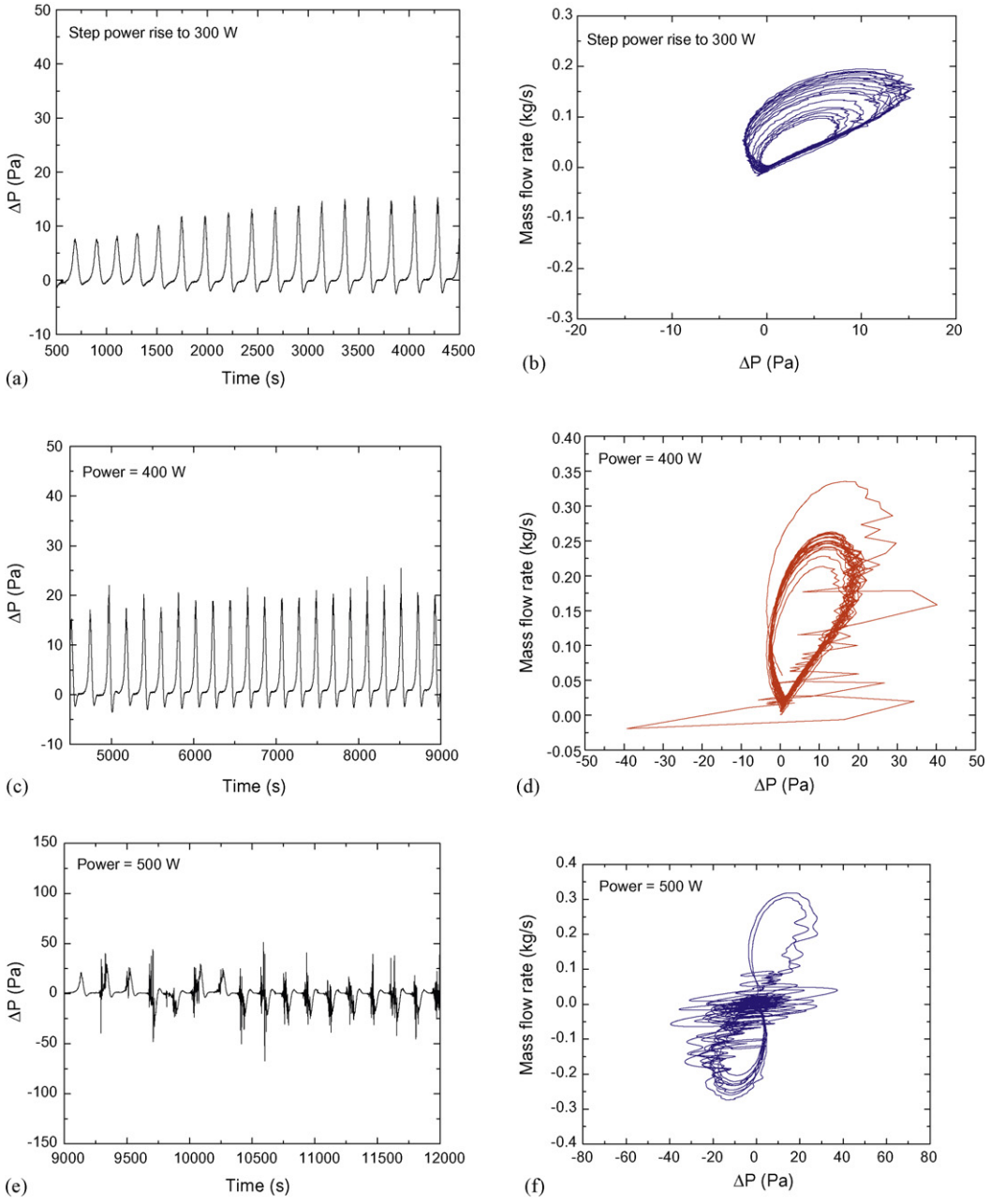

Fig. 9. Flow characteristics of power raising and power set back for start-up at 300 W. (a) Unidirectional pulsing at 300 W, (b) phase plot for unidirectional pulsing at 300 W, (c) unidirectional pulsing at 400 W, (d) phase plot for unidirectional pulsing at 400 W, (e) bidirectional pulsing and chaotic switching at 500 W, (f) phase plot for bidirectional pulsing at 500 W, (g) bidirectional pulsing with subcooled boiling at 600 W, (h) phase plot for bidirectional pulsing with subcooled boiling at 600 W, (i) bidirectional pulsing for power set back to 500 W, (j) phase plot for bidirectional pulsing at power set back to 500 W, (k) unidirectional pulsing at power set back to 400 W and (l) phase plot for unidirectional pulsing at 400 W.

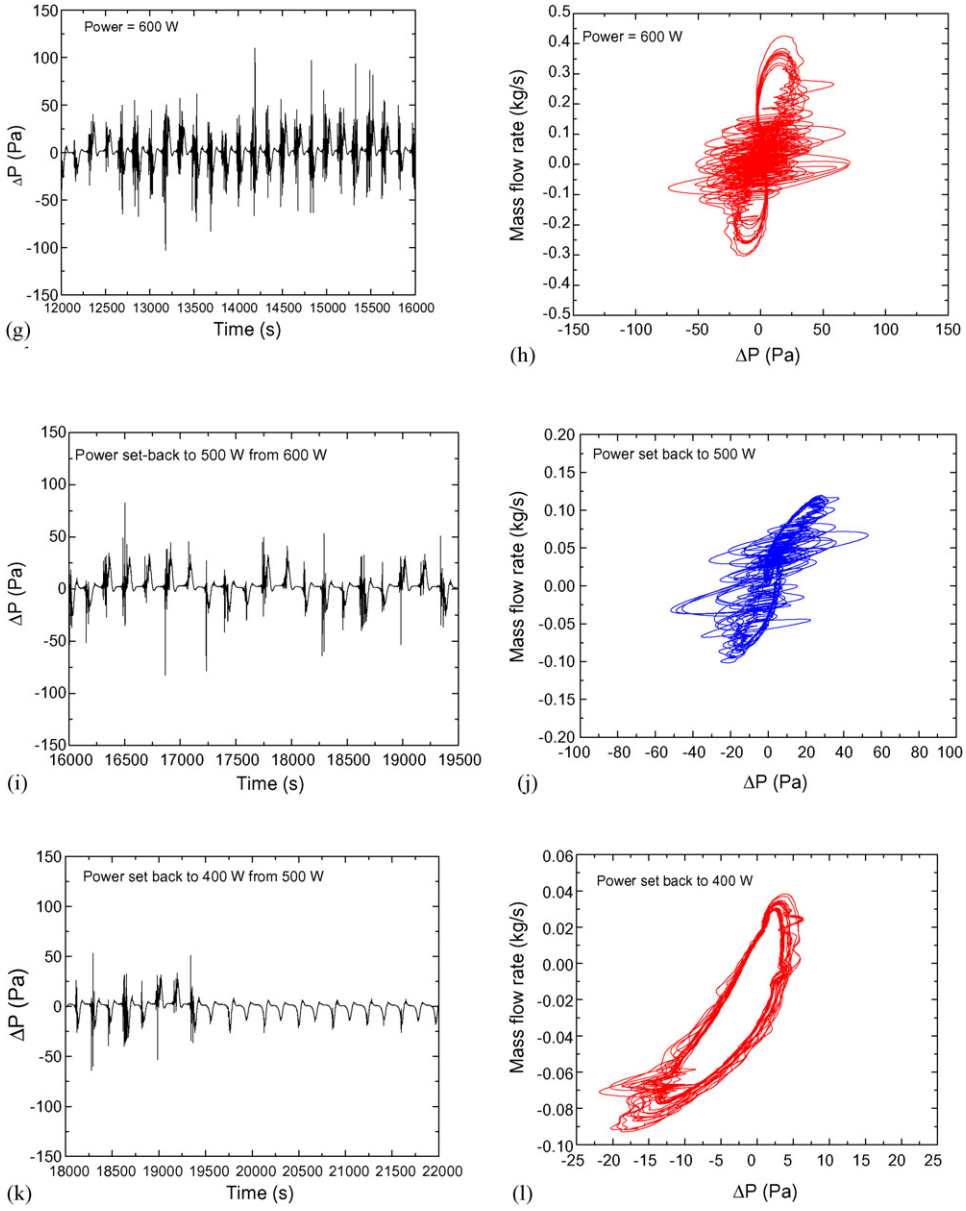

Fig. 9. (*Continued*).

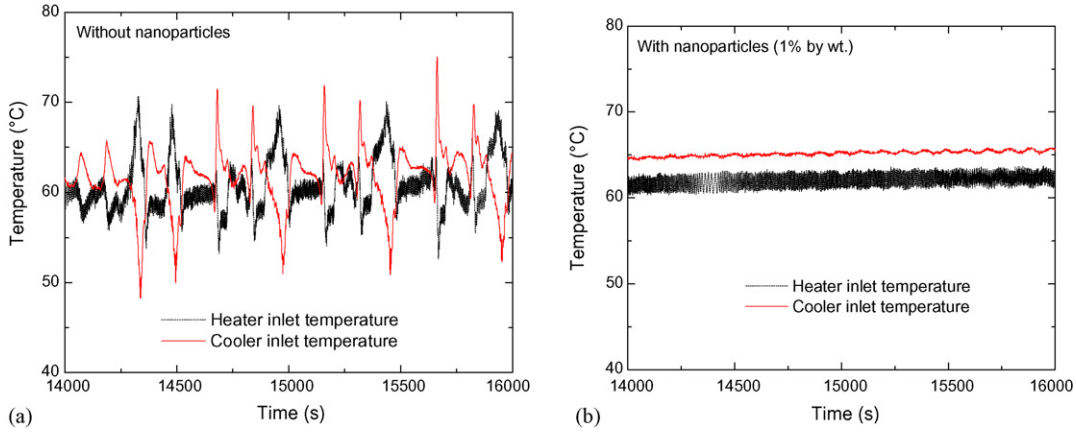

Fig. 10. Comparison of temperature variation at 600 W with water and with nanofluids. (a) Variation of temperature without nanofluids and (b) variation of temperature with nanofluids.

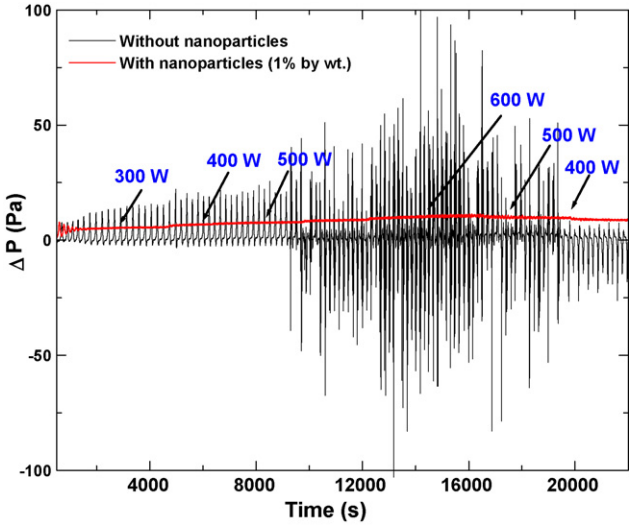

Fig. 11. Suppression of flow instability with nanofluids during power raising and step back process.

rate is increased between 20 and 35% depending on the concentration of nanoparticles and heater power.

3.5.2. Effect of concentration of nanoparticles on stability

The step power rise to 300 W and subsequent power raising–power set back experiments was repeated with different concentration of nanoparticles (0.3–2% by wt.). It was found that the flow instabilities are suppressed even with a low concentration of 0.3% by weight of Al_2O_3 nanoparticles as shown in Fig. 16.

4. Analysis of steady-state data

Prior studies (Vijayan et al., 2001) showed that the steady-state flow in a uniform diameter natural circulation loop with negligible local pressure losses could be expressed as

$$Re_{ss} = C\left[Gr_m \frac{D}{L_t} I_{ss}\right]^r \tag{1}$$

where $I_{ss} = \oint \theta_{ss} dZ$, $C = (2/p)^r$ and $r = 1/(3-b)$ with p and b obtained from a friction factor correlation of the following form:

$$f = \frac{p}{Re^b} \tag{2}$$

The numerical value of the integral $I_{ss} = 1$ for the horizontal heater and horizontal cooler (HHHC) orientation (Vijayan, 2002) so that the steady-state flow is given by

$$Re_{ss} = C\left[Gr_m \frac{D}{L_t}\right]^r \tag{3}$$

If we assume that the temperature variation is linear in the cooler (it may be noted that the heater temperature distribution is linear for a constant heat flux condition), the steady-state flow rate can be calculated by the following expression:

$$Re_{ss} = C\left[(Gr_m)_{\Delta z} \frac{D}{L_t}\right]^r \tag{4}$$

where $(Gr_m)_{\Delta z} = D^3\rho^2\beta g Q_h \Delta z/A\mu^3 C_p$. If we replace H with Δz, the centre line elevation difference, then Eq. (1) can be rewritten as

$$Re_{ss} = C\left[(Gr_m)_{\Delta z} \frac{D}{L_t} \frac{H}{\Delta z} I_{ss}\right]^r \tag{5}$$

Comparing Eqs. (4) and (5), it is easy to show that the error, E, introduced by the assumption of linear variation of temperature in the cooler is given by the following expression:

$$E = \left[\frac{H}{\Delta z} I_{ss}\right]^r \tag{6}$$

If the value of E is unity, then no error is introduced. For HHHC, $\Delta z = H$ and $I_{ss} = 1$, and hence $E = 1$. The steady-state flow rate for can be obtained from the following equations:

$$Re = 0.1768\left((Gr_m)_{\Delta z} \frac{D}{L_t}\right)^{0.5} \text{ for a fully laminar loop } (p = 64 \text{ and } b = 1) \text{ and} \tag{7}$$

$$Re = 1.96\left[(Gr_m)_{\Delta z} \frac{D}{L_t}\right]^{1/2.75} \text{ for a fully turbulent loop } (p = 0.316 \text{ and } b = 0.25) \tag{8}$$

4.1. Testing of the steady-state correlation with present experimental data

From the measured temperature difference across the heater (ΔT_h) and the heater power (Q_h), the steady-state natural circulation mass flow rate, W_{ss}, is obtained as follows:

$$W_{ss} = \frac{Q_h}{C_{p_h}(\Delta T_h)_{ss}} \tag{9}$$

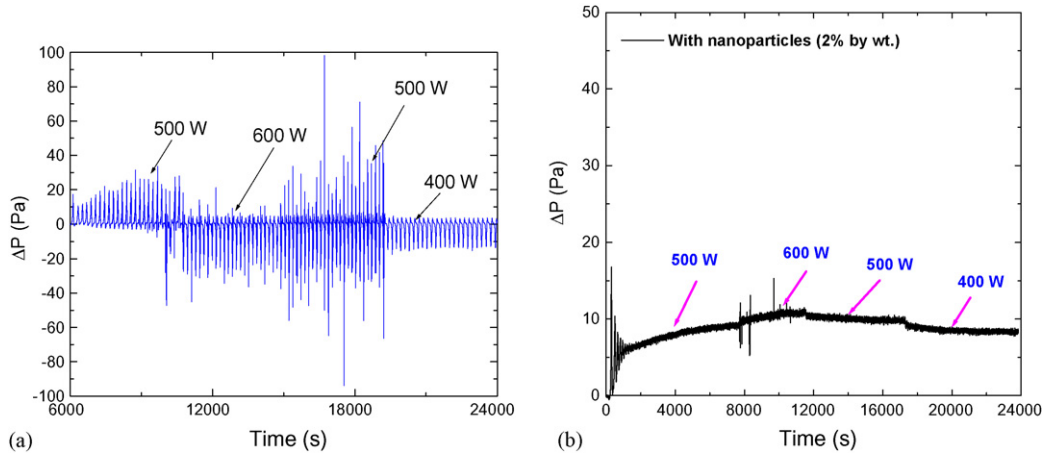

Fig. 12. Comparison of flow behavior with water alone and with nanofluids for start-up at 500 W. (a) Without nanofluids and (b) with nanofluids.

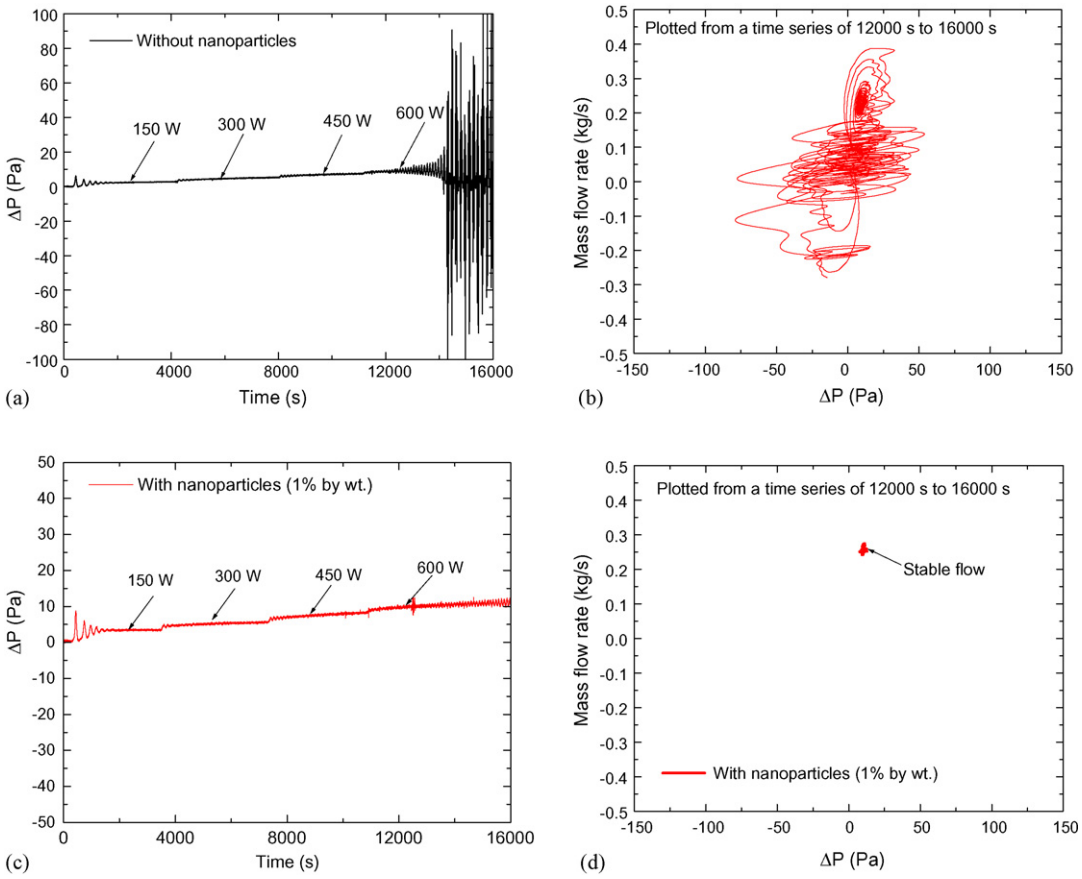

Fig. 13. Comparison of flow behavior with water alone and with nanofluids for gradual increase of power at 150 W up to 600 W. (a) Flow behavior for gradual raising of power with water alone, (b) phase plot for gradual raising of power with water alone, (c) flow behavior for gradual raising of power with nanofluids and (d) phase plot for gradual raising of power with nanofluids.

Using this mass flow rate, the Reynolds number was calculated. Both the *Re* and Gr_m were calculated using the fluid properties estimated at the loop average temperature. The corresponding properties for nanofluids have been calculated using existing models (Buongiorno, 2006) for calculation of *Re* and Gr_m. The steady-state data are compared with the theoretical correlations in Fig. 17. It should be noted that the validity of the above flow formulation (Eqs. (7) and (8)) has already been well established for single-phase natural circulation loops demonstrated by its close agreement with a large number of experimental data obtained from around 25 different loops (Vijayan et al., 2007). For the present loop, the experimental data with water alone are predicted well by the generalized flow correlation whereas there is a large deviation between the model and the experimental data obtained using nanofluids as shown in Fig. 17. This clearly points out the deficiency of existing property models for nanofluids for simulation of natural circulation phenomena.

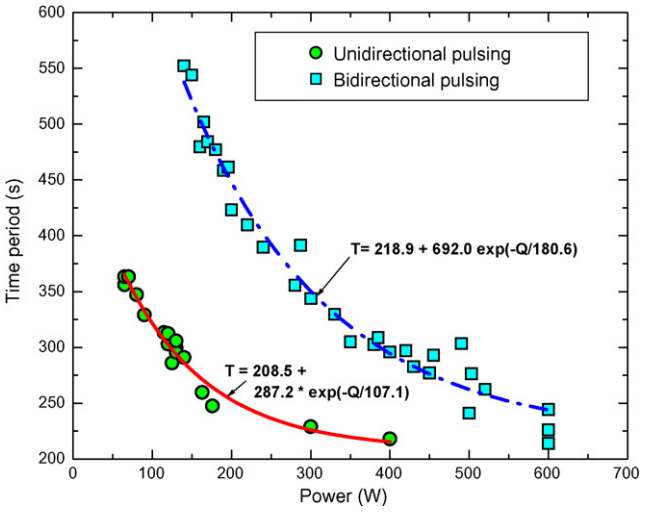

Fig. 14. Variation of time period of oscillation with water alone.

4.2. Possible explanation for suppression of instabilities

With the lack of established data for physical property variation of nanofluids with temperature, it is definitely difficult to discuss the interesting characteristics of natural circulation with nanofluids. However, we have attempted to clarify the reason for suppression of flow instabilities with nanoparticles with the hypothesis of Welander (1967).

According to this, following a thermal disturbance in the system, a hot pocket of fluid may emerge from the heated section slightly hotter than its normal steady-state temperature. This hot pocket while ascending along the hot leg accelerates the flow because of larger buoyancy force thus created. When this hot pocket emerges out from the cooler, its identity is maintained because of the lower residence time due to larger velocity. Thus the hot pocket emerges from the cooler at a higher temperature than its normal steady-state temperature. An opposite phenomena occurs if a cold pocket may emerge from the heater. As the cold pocket ascends along the hot leg and the hot pocket descends along the cold leg, the flow gets decelerated with the result that the hot pocket emerges hotter from

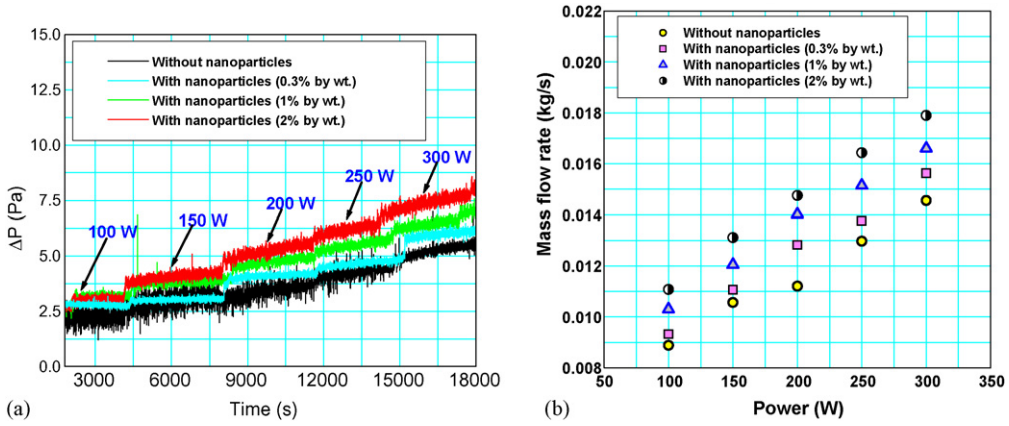

Fig. 15. Comparison of steady-state flow rate with and without nanofluids.

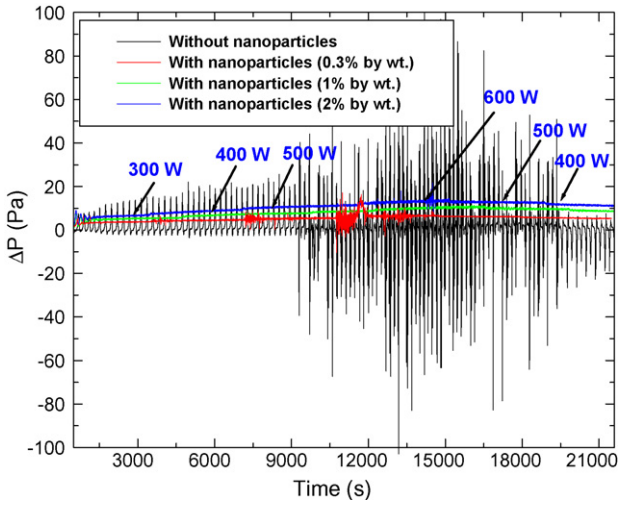

Fig. 16. Effect of concentration of nanoparticles on stability behavior. (a) Variation of flow behavior with different concentration of nanoparticles and (b) variation of steady state flow rate with different concentration of nanoparticles.

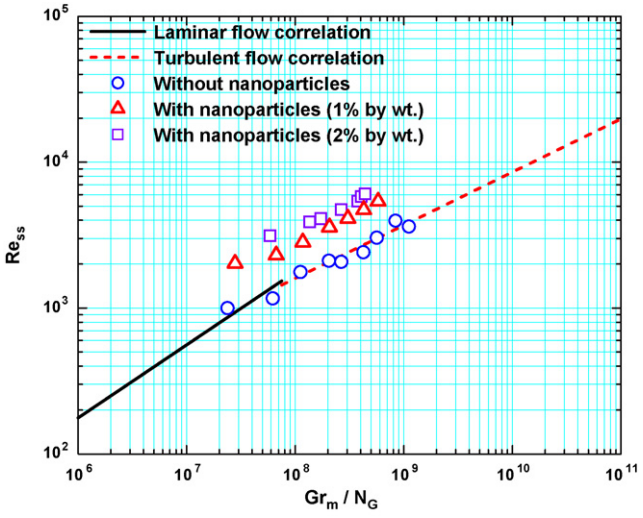

Fig. 17. Variation of steady-state flow rate with different concentration of nanoparticles in non-dimensional plane.

the heater and the cold pocket emerges colder from the cooler with every passing cycle. This amplification process continues until the buoyancy force experiences a reversal in sign causing the flow to reverse. The above-described amplification process then continues in the reverse direction, causing the flow to change its direction repeatedly from clockwise to anticlockwise and vice versa.

Thus, the flow oscillations are mainly due to creation of hot and cold density pockets which get amplified with time in the system. We believe that the significantly increase in natural circulation flow rate due to addition of nanoparticles can dampen the small perturbing forces generated due to hot and cold pockets, which are responsible for sustaining the instabilities. In addition, the time lag among the regenerative feedback effects of flow rate, pressure drop and driving buoyancy force is reduced due to enhanced flow rate, which are the paramount factors for occurrence of flow instabilities. Of course, the enhancement of thermal diffusivity is not significant (hardly less than ~1.74%, calculated using the Murshed et al. Model, 2006); but this also aids in thermally diffusing the hot and cold pockets in addition to the significant momentum diffusion aided by the large flow rate.

5. Conclusions

In this study, we have demonstrated experimentally the interesting thermal–hydraulic characteristics of a single-phase natural circulation loop with different concentration of Al_2O_3 nanoparticles suspended in water. The flow instabilities observed with water is found to be suppressed when a small concentration of nanoparticles was suspended in it. The natural circulation flow was found to increase with nanofluids depending on its concentration.

We have assessed the existing natural convection models for simulation of natural circulation as a function of the system geometry and operating conditions. The models are found to be in good agreement with the steady-state test data with water alone. However, large deviations are found between the models and measurements for nanofluids.

Depending on the heat addition paths and the heater power, the following distinctive unstable flow regimes were observed with water alone:

(1) periodic unidirectional pulsing flow;
(2) chaotic switching between unidirectional and bidirectional pulsing flow;
(3) periodic bidirectional pulsing flow and
(4) Compound instability with the system switching from single-phase to two-phase in every cycle.

However, none of the above flow regime was observed with nanofluids.

Appendix A. 1. Transient flow rate calculation from the measured pressure drop

Assuming incompressible flow across a section of horizontal unheated piping, the transient pressure drop under single-phase condition can be expressed as

$$\Delta P(t) = \frac{L}{A}\frac{dW}{dt} + \frac{fLW^2}{2D\rho A^2} \tag{A-1}$$

Using a friction factor correlation of the form of Eq. (2), the above equation can be rewritten as

$$\Delta P(t) = \frac{L}{A}\frac{dW}{dt} + \frac{pL\mu^b W^{2-b}}{2D^{1+b}\rho A^{2-b}} \tag{A-2}$$

Applying the implicit procedure to the above equation, the transient flow rate can be expressed as

$$W_c + \frac{p\ \Delta t \mu^b W_c^{2-b}}{2D^{1+b}\rho A^{1-b}} = W_p + \frac{A\ \Delta t}{L}\Delta P_c \tag{A-3}$$

where the subscripts c and p refer, respectively to the current and previous time steps. The above equation is a polynomial in W_c (the flow rate at the current instant) which can be solved by a numerical method (bisection or Newton–Raphson method) to obtain the flow rate as a function of time from the measured instantaneous pressure drop. Instrument delays are negligible compared to the response of the process.

Appendix B. 2. Derivation for calculating settling velocity

Considering a force balance on a spherical particle falling through a static fluid and assuming that the total drag acts through the centre of mass,

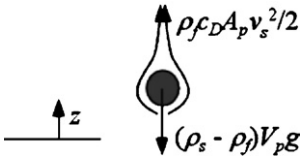

Viscous drag force = gravity force (buoyancy):

$$C_D A_p \frac{1}{2}\rho_f {V_s}^2 = (\rho_p - \rho_f)V_p g \tag{A-4}$$

- V_p = volume of the particle $= \frac{4}{3}\pi(D/2)^3$
- V_s = settling velocity
- $C_D = f(Re_p)$ and $Re_p = \frac{\rho_p V_s D_p}{\mu}$

The drag coefficient's dependence on Re_p is quite complex and somewhat dependent on the shape of the particle. But for small Re_p, the drag coefficient is linearly proportional to Re_p. They are proportional because the flow around the particle does not separate (it is laminar). In this case, potential flow theory describes the flow field and the pressure drop related to the settling particle. From Stokes law for viscous resistance, drag $= 3\pi D_p \mu V_s$

Hence the nanoparticle settling velocity can be calculated as

$$\frac{\pi}{6}D_p^3(\rho_p - \rho_f)g = 3\pi D_p \mu V_s \tag{A-5}$$

$$V_s = \frac{D_p^2(\rho_p - \rho_f)g}{18\mu} \tag{A-6}$$

Appendix C. 3. Calculating fluid velocity

The natural circulation flow velocity can be calculated as follows:

$$W_{ss} = \left[\frac{2}{p}\frac{g\rho_r\beta_T HQD_r^b A_r^{2-b}\rho_l}{\mu_r^b N_G Cp}\right]^{1/(3-b)} \tag{A-7}$$

Hence, fluid velocity

$$V_f = \frac{W_{ss}}{A\rho} \tag{A-8}$$

For the present experiments, the minimum flow velocity has been calculated and found to be 1.71×10^{-2} m/s for the lowest power experiment.

References

Bernier, M.A., Baliga, B.R., 1992. A 1-D/2-D model and experimental results for a closed-loop thermosyphon with vertical heat transfer sections. Int. J. Heat Mass Transf. 35, 2969–2982.

Buongiorno, J., 2006. Convective transport in nanofluids. ASME J. Heat Transf. 128, 240–250.

Chato, J.C., 1963. Natural convection flows in a parallel channel systems. J. Heat Transf. 85, 339–345.

Choi, S.U.S., 1995. Enhancing thermal conductivity of fluids with nanoparticles. ASME FED 231, 99–103.

Creveling, H.F., De Paz Baladi, J.Y., Schoenhals, R.J., 1975. Stability characteristics of a single-phase free convection loop. J. Fluid Mech. 67, 65–84.

Das, S.K., Putra, N., Thiesen, P., Roetzel, W., 2003a. Temperature dependence of thermal conductivity enhancement for nanofluids. J. Heat Transf. Trans. ASME 125, 567–574.

Das, S.K., Putra, N., Roetzel, W., 2003b. Pool boiling characteristics of nano-fluids. Int. J. Heat Mass Transf. 46, 851–862.

Das, S.K., Choi, S.U.S., Patel, H.E., 2006. Heat transfer in nanofluids—a review. Heat Transf. Eng. 27 (10), 3–19.

Daungthongsuk, W., Wongwises, S., 2007. A critical review of convective heat transfer of nanofluids. Renew. Sustain. Energy Rev. 11, 797–817.

Delmastro, D.F., 2000. Thermal–hydraulic aspects of CAREM reactor. In: Proceedings of the IAEA Technical Committee Meeting on Natural Circulation Data and Innovative Nuclear Power Plant Design, Vienna, Austria, July 18–21.

Ho, C.J., Chiou, S.P., Hu, C.S., 1997. Heat transfer characteristics of a rectangular natural circulation loop containing water near its density extreme. Int. J. Heat Mass Transf. 40, 3553–3558.

Holman, J.P., Boggs, J.H., 1960. Heat transfer to freon 12 near the critical state in a natural circulation loop. J. Heat Transf. 82, 221–226.

Huang, B.J., Zelaya, R., 1988. Heat transfer behaviour of a rectangular thermosyphon loop. J. Heat Transf. 110, 487–493.

Kapitaniak, T., 2000. Chaos for Engineers, Theory, Applications and Control, 2nd revised edition. Springer-Verlag, Berlin, pp. 69–86.

Kostic, M., Choi, S.U.S., 2006. Critical issues and application potentials in nanofluids research. In: Proceedings of MN2006, Multifunctional Nanocomposites, Honolulu, Hawaii, September 20–22.

Maxwell, J.C., 1881. A Treatise on Electricity and Magnetism, vol. 1., 2nd ed. Clarendon Press, Oxford, UK.

Misale, M., Tagliafico, L., Tanda, G., 1991. Experiments in a free convection rectangular loop. In: Proceedings of the fourth International Symposium on Transport Phenomena in Heat and Mass Transfer, Sydney, Australia, 14–19 July, pp. 203–211.

Murshed, S.M.S., Leong, K.C., Yang, C., 2006. Determination of the effective thermal diffusivity of nanofluids by the double hot-wire technique. J. Phys. D: Appl. Phys. 39, 5316–5322.

Samoilov, O.B., Kurachenkov, A.V., 1997. Nuclear District heating plants AST-500: present status and prospects for future in Russia. Nucl. Eng. Des. 173, 109–117.

Vijayan, P.K., Date, A.W., 1992. The limits of conditional stability for single-phase natural circulation with throughflow in a figure-of-eight loop. Nucl. Eng. Des. 136, 361–380.

Vijayan, P.K., Nayak, A.K., Pilkhwal, D.S., Saha, D., Venkat Raj, V., 1992. Effect of loop diameter on the stability of single-phase natural circulation in rectangular loops. In: Proceedings of the fifth International Topical Meeting on Reactor Thermalhydraulics, NURETH-5, vol. 1, Salt Lake City, UT, pp. 261–267.

Vijayan, P.K., Bhojwani, V.K., Bade, M.H., Sharma, M., Nayak, A.K., Saha, D., Sinha, R.K., 2001. Investigations on the effect of heater and cooler orientation on the steady state, transient and stability behaviour of single-phase natural circulation in a rectangular loop. External Report No. BARC/2001/E/034, Bhabha Atomic Research Centre, Mumbai, India.

Vijayan, P.K., 2002. Experimental observations on the general trends of the steady state and stability behaviour of single-phase natural circulation loops. Nucl. Eng. Des. 215, 139–152.

Vijayan, P.K., Sharma, M., Saha, D., 2007. Steady state and stability characteristics of single-phase natural circulation in a rectangular loop with different heater and cooler orientations. Exp. Therm. Fluid Sci. 31, 9250–9945.
Vijayan, P.K., Nayak, A.K., Saha, D., Gartia, M.R., 2008. Effect of loop diameter on the steady state and stability behaviour of single-phase and two-phase natural circulation loops. Sci. Technol. Nuc. Inst. 2008, doi:10.1155/2008/672704.
Welander, P., 1967. On the oscillatory instability of a differentially heated loop. J. Fluid Mech. 29, 17–30.